J Therm Anal Calorim (2009) 97:937–943
DOI 10.1007/s10973-009-0193-2

Thermochemical properties of some bis(trifluoromethylsulfonyl)imide based room temperature ionic liquids

Ch. Jagadeeswara Rao · R. Venkata Krishnan · K. A. Venkatesan · K. Nagarajan · T. G. Srinivasan

Received: 5 November 2008 / Accepted: 16 April 2009 / Published online: 19 June 2009

Abstract Three different room temperature ionic liquids (RTILs) namely protonated betaine bis(trifluromethylsulfonyl)imide ([Hbet][Tf_2N]), *N*-butyl-*N*-methylpyrrolidinium bis(trifluromethylsulfonyl)imide ($BMPyTf_2N$) and *N*-methyl-*N*-propylpiperidinium bis(trifluromethylsulfonyl)imide ($MPPiTf_2N$) were synthesized and characterized by CHNS analysis, NMR and FTIR spectroscopy. Heat capacity measurements and thermogravimetric analysis of these RTILs were carried out and the results are reported in this paper.

Keywords Differential scanning calorimetry · Heat capacity · Room temperature ionic liquids · Thermogravimetry

Introduction

Room temperature ionic liquids (RTILs) are novel fluids comprising entirely of ions and are molten at temperatures lower than the boiling point of water [1–3]. Generally they contain a bulky organic cation and an organic or inorganic anion. RTILs have several unique properties such as insignificant vapor pressure, high thermal stability, good electrical conductivity, large electrochemical window, wide liquidus range, high heat capacity etc., which make them suitable candidates for a wide variety of applications. RTILs are being envisaged as alternative to the traditional diluent, n-dodecane, in solvent extraction process [4–8] for nuclear fuel reprocessing. Unusual extraction of metal ions was reported, when RTILs were employed as diluents in conjunction with traditional extractants [4–8]. Moreover, the exceptional property of RTIL namely, wide electrochemical window was exploited in a solvent extraction process to facilitate a new mode of recovery that involve electrodeposition of metals from loaded organic phase [7, 8].

RTILs are also being explored for possible applications in non-aqueous reprocessing as substitutes for high temperature molten salts. RTILs having an electrochemical window as large as 6 V, make it possible to reduce the compounds of actinides and fission products up to their metallic state. Nikitenko et al. [9, 10], studied the spectroscopic and electrochemical aspects of U(IV)-hexachloro complexes in 1-butyl-3-methylimidazolium bis(trifluoromethylsulfonyl) imide and tri-1-butylmethylammonium bis(trifluoromethylsulfonyl)imide and the co-ordination behaviour of Np(IV) and Pu(IV) in $bmimTf_2N$. Bhatt et al. [11] studied the electrochemistry of some lanthanides, La^{3+}, Sm^{3+} and Eu^{3+} in $[R_4X][Tf_2N]$, where X = N, P and As. Chen and Hussey [12] studied the electrochemistry of the most electropositive fission product, Cs^+, at mercury film electrode using tri-1-butylmethylammonium bis(trifluoromethylsulfony)imide ionic liquids. Recently, we have also reported the dissolution behaviour of uranium oxides in a task-specific ionic liquid, protonated betaine bis(trifluoromethylsulfonyl)imide, [Hbet][Tf_2N] [13].

For use in aqueous and non-aqueous reprocessing applications, RTILs should have adequate thermal and radiation stability. Ramos et al. [14] studied the glass transition of imidazolium based RTIL and reported the heat capacity jump during glass transition. Zhang et al. [15, 16] determined the molar heat capacities of 1-butylpyridinium tetrafluoroborate and 1-butyl-3-methylimidazolium tetrafluoroborate using adiabatic calorimeter respectively and

Ch. Jagadeeswara Rao · R. Venkata Krishnan · K. A. Venkatesan · K. Nagarajan (✉) · T. G. Srinivasan
Fuel Chemistry Division, Indira Gandhi Centre for Atomic Research, Kalpakkam 603 102, India
e-mail: knag@igcar.gov.in

reported the enthalpy and entropy change during glass transition of RTIL. Zhang et al. [17] reported some thermodynamic properties of 1-butyl-3-methylimidazolium chloride determined by TG, DTA and DSC. However, the thermal properties of protonated betaine bis(trifluromethylsulfonyl)imide ([Hbet][Tf_2N]), *N*-butyl-*N*-methylpyrrolidinium bis(trifluromethyl-sulfonyl)imide (BMPyTf_2N), *N*-methyl-*N*-propylpiperidinium bis(trifluromethylsulfonyl) imide (MPPiTf_2N) have not been reported so far. Therefore the aim of the present study is to determine the heat capacities and thermogravimetric analysis of these RTILs and report the results in this paper.

Experimental

Materials

All the chemicals used in this study were of analytical reagent grade. *N*-methylpyrrolidine, *N*-methylpiperidine and lithium bis(trifluoromethylsulfonyl)imide were procured from Fluka, and 1-bromobutane and 1-bromopropane from Lancater. Betaine hydrochloride was purchased from Alfa-Aesar.

Synthesis of [Hbet][Tf_2N]

[Hbet][Tf_2N] was prepared by the procedure described elsewhere [18]. It involves a metathesis reaction between betaine hydrochloride (0.1 mole, 25 mL) and Lithium bis(trifluoromethylsulfonyl)imide (0.1 mole, 50 mL) in water as shown in Scheme 1. The solutions were stirred for about an hour and the colourless ionic liquid phase separated was washed few times with distilled water to free the chloride (tested with acidified $AgNO_3$ solution) ion. The product was dried in a rotary evaporator at 343 K for 24 h and stored in a vacuum desiccator. The yield ranged from 75 to 80%. The results of the analysis and the properties determined are: water content 0.57% (by Karl-Fischer titration), melting point 330 K, viscosity 351 cP at 333 K. Elemental analysis yielded (%, theoretical value in parenthesis) C 21.08 (21.11), H 2.90 (3.04), N 6.94 (7.03), S 16.25 (16.10). IR bands: 1200 cm^{-1} C–F asymmetric stretch, 1142 cm^{-1} SO_2 symmetric stretch, 1059 cm^{-1} S–N–S asymmetric stretch, 1739 cm^{-1} C=O stretch, 2964 cm^{-1} O–H stretch, 2835 cm^{-1} C–H stretch. ^{1}H-NMR (500 MHz, d_6-DMSO, TMS): δ 3.265 (s, 3 $\times$ CH_3), 4.289 (s, 2H), 8.245 (s, OH). ^{13}C-NMR (500 MHz, d_6-DMSO, TMS): δ 166.74 (COO), 123.77, 121.21, 118.65, 116.09 (2 $\times$ CF_3), 63.17 (N–CH_2), 53.39 (3 $\times$ CH_3).

Synthesis of *N*-butyl-*N*-methylpyrrolidinium bromide, BMPyBr

The synthesis of BMPyBr is reported elsewhere [19]. In involves drop-wise addition of *N*-butylbromide (54 mL = 0.5 mole) into a solution of *N*-methylpyrrolidine (0.5 mol) in acetonitrile (110 mL) at 273 K. The reaction mixture was stirred for nearly 4 h, and left overnight. It was then dried in a rotary evaporator at 343 K to remove acetonitrile. The yellow colored product, BMPyBr, was purified by treating its solution in water with activated charcoal and stirred for more than 24 h at 338–343 K. The mixture was filtered, and dried again in rotary evaporator at 343 K. The colourless solid, BMPyBr, obtained was further purified by recrystallization from acetonitrile and characterized by various techniques. The yield was 97%. The results of the analysis and the properties are: melting point 530 K. Elemental analysis of BMPyBr yielded (%, theoretical value in brackets) C 47.39 (47.65), H 15.34 (15.2), N 11.71 (11.30). ^{1}H-NMR (500 MHz, $CDCl_3$, TMS): δ 0.963 (t, 3H), 1.431 (q, 2H), 1.721 (m, 2H), 2.267 (m, 4H), 3.253 (m, 4H), 3.629 (t, 2H), 3.802 (s, 3H). ^{13}C-NMR (500 MHz, $CDCl_3$, TMS): δ 64.44 (ring N–CH_2), 64.00 (N–CH_2), 48.70 (2 $\times$ ring CH_2), 25.94 (CH_2), 21.66 (CH_2), 19.74 (CH_2), 13.69 (2 $\times$ CH_3).

Synthesis of BMPyTf_2N

BMPyTf_2N was prepared by metathesis reaction [19], shown in Scheme 2. It involved stirring the aqueous solutions of *N*-butyl-*N*-methylpyrrolidinium bromide (0.1 mol) and lithium bis(trifluoromethylsulfonyl)imide (0.1 mol) at room temperature for 3 h. The colorless ionic liquid phase separated at the bottom was extracted in dichloromethane and washed a couple of times with distilled water to remove the reactants, if any. The solution was dried under rotary evaporator at 343 K for 24 h. The RTIL was transferred into amber colored bottle and stored in vacuum desiccators. The yield was 97%. The results of the analysis and the properties measured are: IR bands: 1193 cm^{-1} C–F asymmetric stretch, 1139 cm^{-1} SO_2 symmetric stretch, 1054 cm^{-1} S–N-S asymmetric stretch, 2881 cm^{-1} C–H stretch, 2970, 2964 cm^{-1} ring C–H stretch, 2179 cm^{-1} ring methylene C–N stretch, 1473, 1353 cm^{-1} methylene and methyl C–N stretch. ^{1}H-NMR (500 MHz, $CDCl_3$, TMS): δ 0.95 (t, 3H), 1.41 (m,2H), 1.73 (m,2H), 2.21 (m, 4H), 3.32 (m, 4H), 3.47 (t, 2H), 3.54 (s, 3H). ^{13}C-NMR (500 MHz, $CDCl_3$, TMS): δ 121.1 (CF_3), 118.55 (CF_3), 64.62 (N–CH_2 ring), 64.42 (N–CH_2), 48.53 (ring CH_2), 48.24 (ring CH_2), 25.74 (CH_2), 21.56 (CH_2), 19.54 (CH_2),

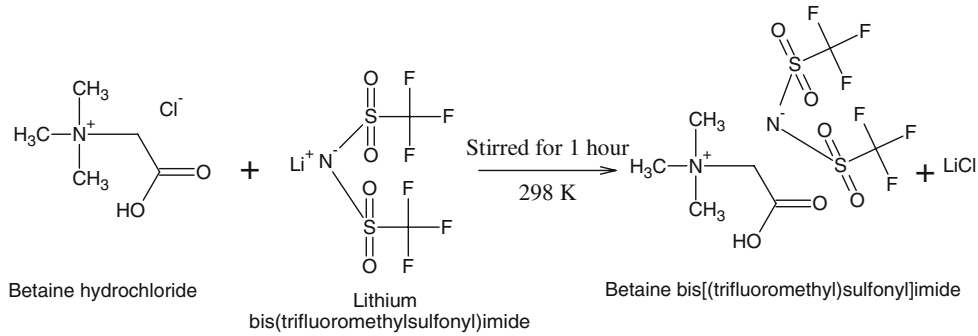

Scheme 1 The reaction scheme used for the synthesis of protonated betaine bis(trifluoromethylsulfonyl)imide

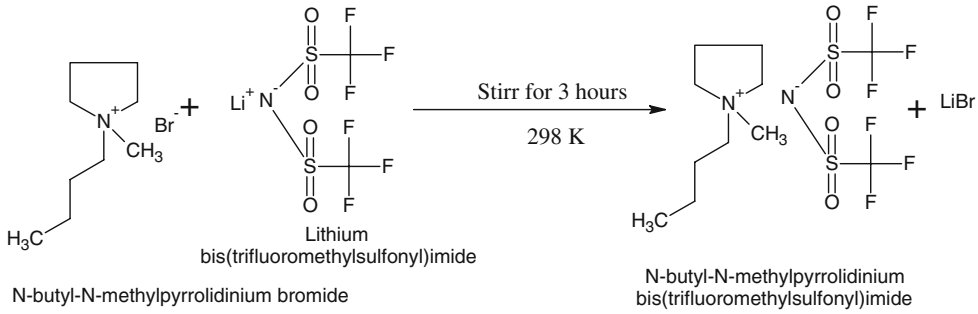

Scheme 2 Reaction scheme used for the synthesis of *N*-butyl-*N*-methylpyrrolidinium bis(trifluoromethylsulfonyl)imide

13.37 (CH_3), 13.13 (CH_3). The water content of the ionic liquid was less than 0.5% (Karl-Fischer titration).

Synthesis of *N*-methyl-*N*-propylpiperidinium bromide, MPPiBr

The synthesis of MPPiBr and MPPiTf_2N is reported elsewhere [20]. A solution of *N*-methylpiperidine (23.5 mL = 0.2 mol) in iso-propanol (76 mL) was added dropwise to 1-bromopropane (18.25 mL = 0.2 mole) under stirring at 273 K. The solution was stirred for about two hours and a pale yellow colored solid, *N*-methyl-*N*-propylpiperidinium bromide, was separated. It was purified by treating its aqueous solution with activated charcoal and stirred for about 10 h at 333–343 K. Yield: 95%, melting point: 523 K, Elemental analysis of MPPiBr yielded (%, theoretical value in brackets) C 48.28 (48.65), H 13.62 (13.8), N 6.85 (6.53). ^{1}H-NMR (500 MHz, $CDCl_3$, TMS): δ 0.979 (t, 3H), 1.740 (m, 4H), 1.846 (m, 4H), 3.262 (s, 3H), 3.578 (m, 4H), 3.674 (m, 2H); ^{13}C-NMR (500 MHz, $CDCl_3$, TMS): δ 64.62 (cyclic CH_2), 60.87 (2 × cyclic CH_2), 48.22 (2 × cyclic N–CH_2), 20.55 (N–CH_2), 20.16 (CH_2), 15.51(CH_3), 10.80 (CH_3).

Synthesis of MPPiTf_2N

The procedure for the preparation of MPPiTf_2N is illustrated in Scheme 3. It involved mixing the aqueous solutions of *N*-methyl-*N*-propylpiperidinium bromide (0.1 mol) and lithium bis(trifluoromethylsulfonyl)imide (0.1 mol) for about 1 h. The RTIL phase settled at bottom was extracted into dichloromethane and washed a couple of times with equal volume of distilled water. The organic phase was dried under rotary evaporator at 343 K. The liquid phase obtained was covered with a black sheet and stored in vacuum desiccator. Yield: 90%. IR bands: 1193 cm^{-1} C–F asymmetric stretch, 1139 cm^{-1} SO_2 symmetric stretch, 1054 cm^{-1} S–N–S asymmetric stretch, 2881 cm^{-1} C–H stretch, 2970, 2964 cm^{-1} ring C–H stretch, 2179 cm^{-1} ring methylene C–N stretch, 1473, 1353 cm^{-1} methylene and methyl C–N stretch. ^{1}H-NMR (500 MHz, $CDCl_3$, TMS): δ 1.028 (m, 3H), 1.749 (m, 4H), 1.891(s, 4H), 3.008 (m, 3H), 3.252 (m, 2H), 3.328(m, 4H); ^{13}C-NMR (500 MHz, $CDCl_3$, TMS): δ 123.7(cyclic CH_2), 121.14(CF_3), 118.59(CF_3), 116.03(cyclic CH_2), 65.68(cyclic CH_2), 61.41(cyclic N–CH_2), 47.8 (cyclic N–CH_2), 20.66(N–CH_2), 19.81(CH_2), 15.32(CH_3), 10.42(CH_3). The water content of the ionic liquid was less than 0.5% (Karl-Fischer titration).

Structural characterization

NMR analysis of the RTILs were done using Bruker AVANCE III 500 MHz (AV 500) multi nuclei solution NMR. Microelemental CHNS analysis of TSIL was carried out by using Elementer Vario EL. IR spectra was recorded using Bomem FTIR spectrometer model—103.

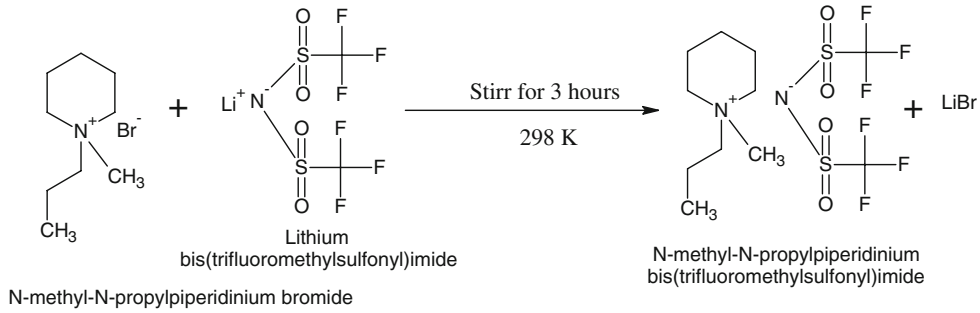

Scheme 3 Reaction scheme used for the synthesis of *N*-methyl-*N*-propylpiperidinium bis(trifluoromethylsulfonyl)imide

Thermogravimetric (TG) analysis

The samples of [Hbet][Tf_2N], BMPyTf_2N and MPPiTf_2N were subjected to thermogravimetric analysis in the temperature range 298–1300 K to determine the decomposition temperatures using thermogravimetric analyzer model number TGA/SDTA 851e of M/s. Mettler Toledo GmbH, Switzerland. Temperature calibration was carried out by determining the melting temperatures of pure In, Sn and Au samples. Ultra high pure argon was used as purge gas at a flow rate of 10 mL min^{-1}. The heating rate of 10 K min^{-1} was used during the measurement.

Differential scanning calorimetry

A heat flux type differential scanning calorimeter (model number DSC821e/700 of M/s. Mettler Toledo GmbH, Switzerland) was used for the heat capacity measurements. The procedure used for temperature, heat, thermal-lag and heat rate calibrations have been described elsewhere [21]. Ultra high pure argon was used as purge gas at a flow rate of 50 mL min^{-1}.

Heat capacity measurements on RTILs were carried out using a three segment heating program, described elsewhere [21]. Each heat capacity measurement consisted of a set of three runs, a blank run with empty pans on both sample and reference sides, a calibration run with empty pan on the reference side and the pan with disc of sapphire on the sample side and finally a sample run with empty pan on the reference side and the pan with sample on the sample side. The sample was pre-heated at 423 K for about half an hour in the DSC cell before the measurement to remove absorbed moisture, if any. The weight of the sample after the completion of the experiment was taken for the calculation of heat capacity.

Results and discussions

The derivative thermogravimetric patterns (DTG) of [Hbet][Tf_2N], BMPyTf_2N and MPPiTf_2N are shown in Fig. 1. It can be seen that MPPiTf_2N and BMPyTf_2N undergo single step decomposition, while [Hbet][Tf_2N] undergoes two-step decomposition, perhaps due to the presence of –COOH group in the cationic part of [Hbet][Tf_2N]. The DTG patterns indicate that the RTILs,

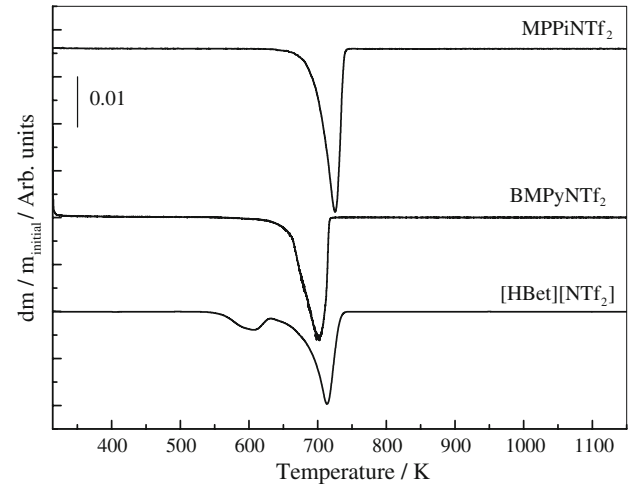

Fig. 1 The derivative thermogravimetric patterns (DTG) of [Hbet][Tf_2N], BMPyTf_2N and MPPiTf_2N

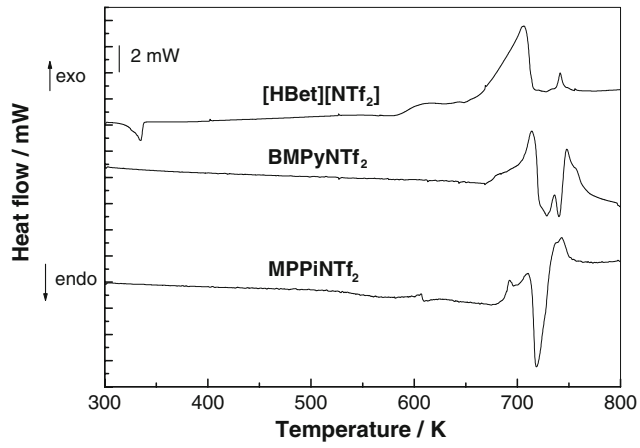

Fig. 2 The DSC scans of [Hbet][Tf_2N], BMPyTf_2N and MPPiTf_2N

Table 1 Thermodynamic functions of [Hbet][Tf_2N]

T (K)	$C_{p,m}$ (J K^{-1} mol^{-1})		$H_T^0 - H_{298}^0$ (J mol^{-1})	$S_T^0 - H_{298}^0$ (J K^{-1} mol^{-1})
	Measured	Fit		
340	585	585	24353	77
350	589	587	30204	94
360	589	589	36074	110
370	592	591	41965	126
380	594	593	47875	142
390	595	596	53805	158
400	598	598	59757	173
410	601	600	65729	187
420	603	602	71724	202
430	606	605	77742	216
440	609	607	83783	230
450	609	610	89849	244
460	612	613	95940	257
470	617	615	102058	270

Table 2 Thermodynamic functions of $BMPyTf_2N$

T (K)	$C_{p,m}$ (J K^{-1} mol^{-1})		$H_T^0 - H_{298}^0$ (J mol^{-1})	$S_T^0 - H_{298}^0$ (J K^{-1} mol^{-1})
	Measured	Fit		
298	606	606	0	0
300	608	608	1214	4
310	619	619	7350	24
320	628	628	13585	44
330	637	637	19914	63
340	645	646	26333	83
350	656	655	32840	101
360	664	663	39431	120
370	672	671	46104	138
380	680	679	52855	156
390	687	687	59684	174
400	693	694	66588	192
410	702	701	73565	209
420	708	708	80613	226
430	716	715	87732	243
440	723	722	94920	259
450	726	729	102175	275
460	738	736	109497	291
470	743	742	116885	307
480	745	748	124337	323
490	752	755	131853	339
500	760	761	139432	354
510	769	767	147074	369
520	776	773	154777	384

$MPPiTf_2N$, $BMPyTf_2N$, are thermally stable up to 650 K, however the onset of decomposition of [Hbet][Tf_2N] occurs at 560 K.

Table 3 Thermodynamic functions of $MPPiTf_2N$

T (K)	$C_{p,m}$ (J K^{-1} mol^{-1})		$H_T^0 - H_{298}^0$ (J mol^{-1})	$S_T^0 - H_{298}^0$ (J K^{-1} mol^{-1})
	Measured	Fit		
298	607	607	0	0
300	608	608	1215	4
310	615	615	7329	24
320	622	621	13511	44
330	628	628	19758	63
340	634	635	26073	82
350	642	641	32454	101
360	647	648	38901	119
370	655	655	45415	137
380	661	661	51995	154
390	669	668	58641	171
400	675	675	65354	188
410	681	681	72133	205
420	687	688	78978	222
430	695	694	85889	238
440	700	701	92866	254
450	709	708	99910	270
460	715	714	107019	285
470	721	721	114195	301
480	726	727	121436	316
490	734	734	128744	331
500	742	741	136117	346
510	744	747	143557	361
520	756	754	151062	375

DSC measurements were carried out at different heating rate viz. 2, 5 and 10 $K.min^{-1}$. The variation observed in the melting points obtained at these heating rates is within ± 1 K and that in decomposition temperature is within ± 2 K. The DSC scans of all the three samples are shown in Fig. 2. [Hbet][Tf_2N] is a solid and $BMPyTf_2N$ and $MPPiTf_2N$ are liquids at ambient temperature. The DSC scan of [Hbet][Tf_2N] results in an endothermic peak at 340 K corresponding to the melting transition. The enthalpy of melting of [Hbet][Tf_2N] is computed to be 30.3 J g^{-1}. The onset of decomposition of [Hbet][Tf_2N], $BMPyTf_2N$ and $MPPiTf_2N$ occur at 580, 670 and 680 K, respectively. The decomposition temperatures obtained using DSC are in good agreement with those obtained by thermogravimetry.

Heat capacity measurements on [Hbet][Tf_2N] were carried out in the temperature range 340–470 K, where as that of $MPPiTf_2N$ and $BMPyTf_2N$ were carried out from 298 to 520 K. The heat capacity data of [Hbet][Tf_2N], $MPPiTf_2N$ and $BMPyTf_2N$ computed as the mean of 10 independent measurements are given in Tables 1, 2, and 3, respectively along with the values for other thermodynamic

Table 4 Equations for determining enthalpy and entropy

S. No	Compound	$H_T^0 - H_{298}^0$	$S_T^0 - H_{298}^0$
1	[Hbet][Tf_2N]	7.09×10^2 (T) − 2.6637×10^{-1} (T^2) − 3.9226×10^6 (T^{-1}) + 2.633×10^{-4}(T^3) − 1.8143×10^5	7.09×10^2 (lnT) − 5.3274×10^{-1}(T) − 1.9613×10^6 (T^{-2}) + 3.95×10^{-4} (T^2) + 4.185×10^3
2	BMPyTf_2N	5.35×10^2 (T) + 2.549×10^{-1}(T^2) + 7.1206×10^6 (T^{-1}) − 2.0585×10^5	5.34×10^2 (lnT) + 5.0982×10^{-1}(T) + 3.5603×10^6(T^{-2}) − 3.237×10^3
3	MPPiTf_2N	4.12×10^2 (T) + 3.288×10^{-1}(T^2) + 1.4362×10^5 (T^{-1}) − 1.5258×10^5	4.12×10^2 (lnT) + 6.5763×10^{-1}(T) + 7.1810×10^4 (T^{-2}) − 2.5462×10^3

Table 5 Fitting equations of the measured heat capacity data

S. No	Compound	Fit equation (J K^{-1} mol^{-1})	Standard deviation (%)	Standard error J K^{-1} mol^{-1}
1	[Hbet][Tf_2N]	709.002 − 5.3274×10^{-1} (T/K) − 3.922592×10^6 $(K/T)^2$ + 0.00079 $(T/K)^2$ (340 − 470 K)	1–3	1.0
2	BMPyTf_2N	534.64 + 0.50982 (T/K) − 7120644.32 $(K/T)^2$ (298–520 K)	1–3	1.7
3	MPPiTf_2N	412.43 + 0.65763 (T/K) − 143620.54 $(K/T)^2$ (298–520 K)	1–3	1.2

functions. The relative standard deviations among the present measurements are in the range of 1–3%. The equations used for determining the thermodynamic functions, H_T^o–H_{298}^o and S_T^o–S_{298}^o, are shown in Table 4. The fit equations for the heat capacity of [Hbet][Tf_2N], MPPiTf_2N and BMPyTf_2N, the standard errors of the fit and the standard deviations among the measurements are also given in Table 5. The measured heat capacity values along with the fit of [Hbet][Tf_2N], MPPiTf_2N and BMPyTf_2N are given in Fig. 3. As can be seen in Fig. 3, the difference in the heat capacity values between MPPiTf_2N and BMPyTf_2N are very less (± 2%). This phenomenon is expected, as MPPiTf_2N and BMPyTf_2N are isomers. There is only a minor structural difference between MPPiTf_2N in which the methylene (–CH_2–) forms a part of a six-membered heterocyclic ring whereas an alkyl group (*n*-butyl) attached to a five-membered heterocyclic ring in BMPyTf_2N. The observed heat capacity of [Hbet][Tf_2N] is much lower than that of MPPiTf_2N and BMPyTf_2N as the total number of bonds in [Hbet][Tf_2N] are lower than that of MPPiTf_2N and BMPyTf_2N.

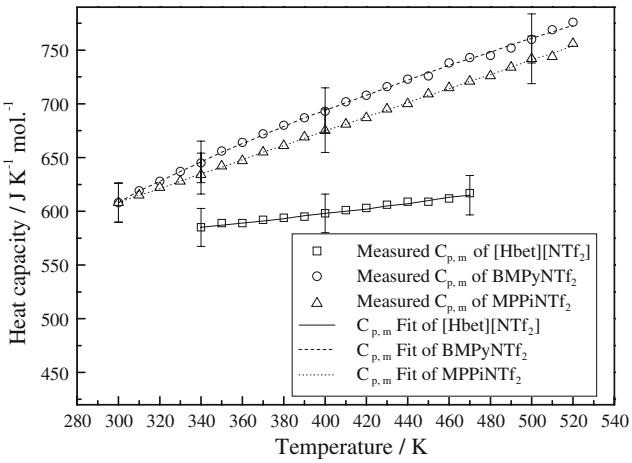

Fig. 3 The measured heat capacity values along with the fit of [Hbet][Tf_2N], BMPyTf_2N and MPPiTf_2N

Summary

MPPiTf_2N and BMPyTf_2N are thermally stable up to 650 K, whereas [Hbet][Tf_2N] is stable only up to 560 K**.** The heat capacity of MPPiTf_2N and BMPyTf_2N are very close (±2%), as these are isomers whereas the heat capacity of [Hbet][Tf_2N] is much lower than that of the others. The present measurements are the first data on the heat capacity of [Hbet][Tf_2N], MPPiTf_2N and BMPyTf_2N.

Acknowledgement The authors wish to thank Mrs. K. V. Syamala, Chemistry Group, IGCAR and SAIF, IITM, Chennai for Karl-Fischer analysis and NMR analysis respectively.

References

1. Welton T. Room-temperature ionic liquids. Solvents for synthesis and catalysis. Chem Rev. 1999;99:2071−84.
2. Earle MJ, Seddon KR. Ionic liquids. Green solvents for the future. Pure Appl Chem. 2000;72:1391−98.
3. Galinski M, Lewandowski A, Stepniak I. Ionic liquids as electrolytes. Electrochim Acta. 2006;51:5567−80.
4. Visser AE, Swatloski RP, Reichert WM, Griffin ST, Rogers RD. Traditional extractants in non-traditional solvents: group 1 and 2 extraction by crown ethers in room temperature ionic liquids. Ind Eng Chem Res. 2000;39:3596−604.

5. Dai S, Ju YH, Barnes CE. Solvent extraction of strontium nitrate by crown ether using room-temperature ionic liquids. J Chem Soc Dalton Trans. 1999:1201−2.
6. Chun S, Dzyuba SV, Bartsch RA. Influence of structural variation in room-temperature ionic liquids on the selectivity and efficiency of competitive alkali metal salt extraction by a crown ether. Anal Chem. 2001;73:3737−41.
7. Giridhar P, Venkatesan KA, Subramaniam S, Srinivasan TG, Vasudeva Rao PR. Extraction of uranium (VI) by 1.1 M tri-N-butylphosphate/ionic liquid and the feasibility of recovery by direct electrodeposition from organic phase. J Alloys Comps. 2008;448:104−8.
8. Giridhar P, Venkatesan KA, Subramaniam S, Srinivasan TG, Vasudeva Rao PR. Electrochemical behavior of uranium (VI) in 1-butyl-3-methylimidazolium chloride and in 0.05 M aliquat-336/chloroform. Radiochim Acta. 2006;94:415−20.
9. Nikitenko SI, Cannes C, Le Naour C, Moisy P, Trubert D. Spectroscopic and electrochemical studies of U(IV)-hexachloro complexes in hydrophobic room-temperature ionic liquids [BuMeIm][Tf_2N] and [$MeBu_3N$][Tf_2N]. Inorg Chem. 2005;44:9497−505.
10. Nikitenko SI, Hennig C, Grigoriev MS, Le Naour C, Cannes C, Trubert D. Structural and spectroscopic studies of the complex [BuMeIm]$_2$[UCl_6] in the solid state and in hydrophobic room temperature ionic liquid [BuMeIm][Tf_2N]. Polyhedron. 2007;26:3136−42.
11. Bhatt AI, May I, Volkovich VA, Hetherington ME, Lewin B, Thied RC, et al. Group 15 quaternary alkyl bistriflimides: ionic liquids with potential application in electropositive metal deposition and as supporting electrolytes. J Chem Soc Dalton Trans. 2002:4532−4.
12. Chen Po-Yu, Hussey CL. Electrodeposition of cesium at mercury electrodes in the tri-1-butylmethylammonium bis((trifluoromethyl) sulfonyl)imide room temperature ionic liquid. Electrochim Acta. 2004;49:5125−38.
13. Jagadeeswara Rao Ch, Venkatesan KA, Nagarajan K, Srinivasan TG. Dissolution of Uranium oxides and electrochemical behavior of U(VI) in task specific ionic liquid. Radiochim Acta. 2008;96:403−9.
14. Moura Ramos JJ, Afonso CAM, Branco LC. Glass transition relaxation and fragality in two Room temperature ionic liquids. J. Therm Anal Calorim. 2003;71:659−66.
15. Zhang ZH, Tan ZC, Li YS, Sun LX. Thermodynamic investigation of room temperature ionic liquid—Heat capacity and thermodynamic functions of $BMIBF_4$. J Therm Anal Calorim. 2006;85:551−7.
16. Zhang ZH, Sun LX, Tan ZC, Xu F, Lu XC, Zeng JL, et al. Thermodynamic investigation of room temperature ionic liquid—Heat capacity and thermodynamic functions of $BPBF_4$. J Therm Anal Calorim. 2007;89:289−94.
17. Zhang M, Kamavaram V, Reddy RG. Thermodynamic properties of 1-butyl-3-methylimidazolium chloride (C_4mim[Cl]) ionic liquid. J Phase Equilib Diffus. 2005;26:124−30.
18. Nockemann P, Thijs B, Pittois S, Thoen J, Glorieux C, Hecke KV. Task-specific ionic liquid for solubilizing metal oxides. J Phys Chem B. 2006;110:20978−92.
19. MacFarlane DR, Meakin P, Sun J, Amini N, Forsyth M. Pyrrolidinium imides: a new family of molten salts and conductive plastic crystal phases. J Phys Chem. 1999;103:4164−70.
20. Sakaebe H, Matsumoto H. N-methyl-N-propylpiperidinium bis(trifluoromethanesulfonyl)imide (PP13–TFSI)—novel electrolyte base for Li battery. Electrochem Comm. 2003;5:594−8.
21. Venkata Krishnan R, Nagarajan K, Vasudeva Rao PR. Heat capacity measurements on $BaThO_3$ and $BaCeO_3$. J Nucl Mater. 2001;299:28−31.